NMR study of trialuminide intermetallics

Chin-Shan Lue,* Suchitra Chepin, James Chepin, and Joseph H. Ross, Jr.†
Department of Physics, Texas A&M University, College Station, Texas 77843-4242
(Received 7 July 1997)

We present a systematic study of the DO_{22}-structure trialuminide intermetallic alloys using ^{27}Al NMR spectroscopy. The quadrupole splittings, Knight shifts, and spin-lattice relaxation times on Al_3Ti, Al_3V, Al_3Nb, and Al_3Ta have been identified. Knight-shift tensors were isolated by observation of quadrupole satellite lines and fitting to the central-transition powder patterns. The results are associated with the local electronic density of states for each crystallographic site. Universally small isotropic Knight shifts and long T_1's are consistent with low Fermi-surface densities of states indicating the importance of Fermi-surface features for the phase stability of these alloys. Larger anisotropic Knight shifts occurring at aluminum site I indicate strong hybridization at this site, and the electric-field-gradient tensors confirm the strong ab plane bonding configuration. Local-moment magnetism is found in Al_3V, yet electrically this material appears very similar to the other DO_{22} aluminides. [S0163-1829(98)07112-4]

I. INTRODUCTION

Trialuminide intermetallic compounds Al_3X are of interest for potential aerospace applications because of their low densities, high melting points, and large elastic moduli. However, their poor ductility at low temperatures has still to be improved. Hence, the possible mechanisms driving the atomic ordering have attracted a large number of studies,[1–5] focused on electronic properties in these related alloys, to understand their structural phase stability.

Of Al_3X alloys (where X is the early-transition element, Sc, Ti, V, Zr, Nb...), the possible crystal structures are Ll_2, DO_{19}, DO_{22}, as well as DO_{23}.[6] For Al_3Ti, Al_3V, Al_3Nb, and Al_3Ta, the ground state DO_{22} is energetically favored. Electronic structure calculations have been performed to understand the stable structures in some of these alloys.[7–10] The calculated total density of states (DOS) exhibited a deep valley at the Fermi level in the DO_{22} structure, attributed to hybridization between Al-p and X-d playing an important role for the DOS reduction. Nevertheless, there has been little quantitative work associated with the local properties in these materials, essential to interpret their structural stability.

Nuclear magnetic resonance (NMR) can be used as an atomic probe in metallic alloys yielding information on site occupation and Fermi-surface features. The present study is concerned with the quadrupole interactions, Knight shifts, and nuclear spin-lattice relaxation in Al_3X alloys as related to the local electronic characteristics. In Al_3X alloys, as shown in Fig. 1, there are two inequivalent crystallographic Al sites in the DO_{22} structure denoted as site I and site II, respectively. Al site I is surrounded by four first-nearest transition element neighbors in the (001) plane, while site II interacts with two in the (100) and two in the (010) planes. The (100), (010), and (001), planes are not equivalent in DO_{22} due to noncubic symmetry. With the study of interactions from different sites, the results can be used to examine the directional bonding between Al and transition elements. On this basis, one can qualitatively understand the brittle nature of the Al_3X alloys in DO_{22}.

II. EXPERIMENT

The samples studied here were prepared from 99.9% Al, 99.99% Ti, 99.7% V, 99.9% Nb, and 99.9% Ta by mixing appropriate amounts of elemental metals, pressing the mixtures into small pellets, and melting them in an Ar arc furnace. The loss of weight upon melting were small and had little effect on the NMR experiments. The resulting ingots were annealed in vacuum-sealed (10^{-5} torr) quartz tubes at 900 °C for about 14 h. In a powder x-ray analysis of the Al_3Ti sample, the six strongest reflections could be indexed according to the expected DO_{22} structure, even on the unannealed sample. Three faint reflections disappeared in the anneal, leaving one unidentified peak with very weak intensity. An x-ray analysis was not carried out for the other compounds, but the NMR signals for all materials changed little in the annealing process, and our NMR spectra (below) reveal clearly that all materials are well-ordered in DO_{22}, with two Al sites as expected. Ordering is accomplished very readily in these materials, since the ordered phases extend nearly to the melt.[11] The alloys, which tend to be brittle, were ground to powder. Samples mixed with granular KBr were placed in plastic vials that showed no observable ^{27}Al NMR signal.

The measurements were taken using a 9-T home-built pulse NMR spectrometer described elsewhere[12] and ^{27}Al signals were observed around 99 MHz. Central transition

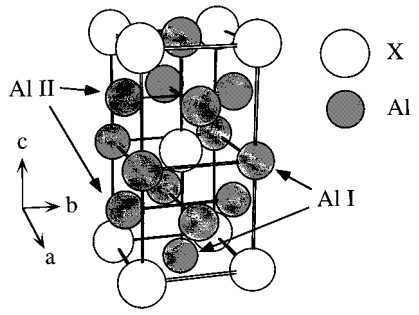

FIG. 1. Crystal structure for the DO_{22}-structure trialuminide intermetallics.

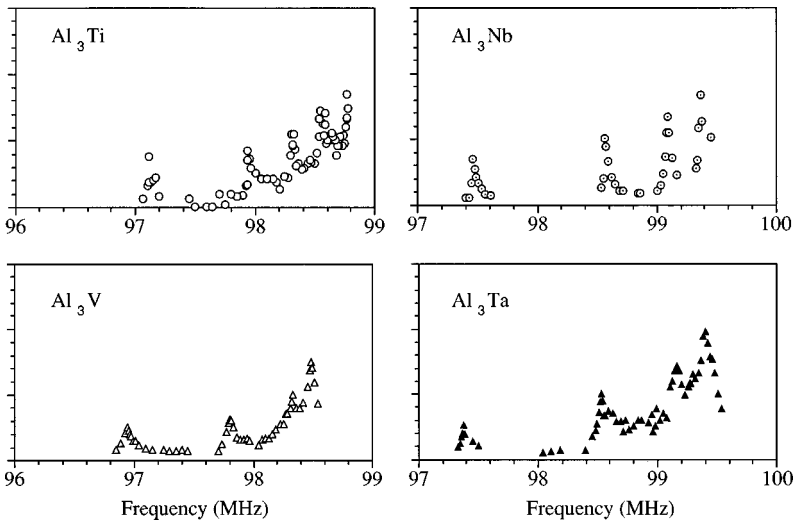

FIG. 2. Lower half of ^{27}Al NMR satellite lines for Al_3Ti, Al_3V, Al_3Nb, and Al_3Ta.

line shapes were obtained from spin echo fast Fourier transforms using a composite-pulse sequence. Wide-line satellite spectra were mapped out by spin echo integration. Previous studies of ordered and disordered Cu-Au alloys have been performed using the same technique.[13] The Knight shifts here were referred to the ^{27}Al resonance frequency of one molar aqueous $AlCl_3$.

III. QUADRUPOLE INTERACTION AND KNIGHT SHIFT

Line shapes for ^{27}Al NMR in these materials are determined by two factors: electric quadrupole interactions with electric-field gradients (EFG's) in the crystals, and magnetic interactions with conduction electrons that provide Knight shifts. For powdered samples, as in our experiment, these lines appear as powder patterns, with distinctive edge structures corresponding to the quadrupole parameters. Due to electric quadrupole coupling, the ^{27}Al NMR spectra ($I=\frac{5}{2}$) are composed of five transition lines per site, so that two inequivalent Al sites in DO_{22} result in 10 lines. Figure 2 displays the low half of the satellite lines for all alloys. The four edge singularities in each spectrum correspond to the $m=-\frac{1}{2}\leftrightarrow-\frac{3}{2}$ and $m=-\frac{3}{2}\leftrightarrow-\frac{5}{2}$ transitions for each of two Al sites in DO_{22}. Since the first-order quadrupole shift is the main effect shaping the satellite line and site symmetries in these crystals are axial, the quadrupole frequency ν_q was determined using these lines. Results are summarized in Table I.

From ν_q for each Al site, we can determine the electric-field gradient (EFG), which arises from the noncubic arrangement of the charged lattice ions and the nonuniform charge density of the conduction electrons due to orbital motion. The EFG for ^{27}Al first neighbors to dilute Ti atoms dissolved in FCC Al metal is known to be $\nu_q=0.67$ MHz.[14] From this a first estimate of Al EFG's in DO_{22} aluminides may be obtained, since the DO_{22} structure is based on an FCC lattice: Al site I is centered between four first-neighbor transition atoms in the ab plane. A simple superposition of the Ti dilute-neighbor EFG for these four atoms gives an axial EFG with $\nu_q=1.34$ MHz. Similarly, a superposition of the EFG's for dilute Ti on the four FCC sites corresponding to the near neighbors of Al site II (Fig. 1) yields an axial EFG with $\nu_q=0.67$ MHz. Compared to FCC Al metal, the DO_{22} structure for all four materials is compressed in the ab plane, and expanded along the c direction, so that an enhancement of the site I EFG and a small reduction of the site II EFG can be expected, compared to the simple model above.

Measured values for Al_3Ti site I and site II are $\nu_q=1.664$ and 0.495 MHz, respectively. The other materials also exhibit similar values (Table I). Based on the argument given above, we assign the NMR site with the largest EFG to site I. Attempts to reproduce the observed EFG's with a point-charge model were unsuccessful. For instance, scaling the Al-Ti dilute values by r^{-3} to account for the ab plane compression in going from FCC Al to Al_3Ti (2.72 versus 2.864 Å) yields $\nu_q=1.56$ MHz, closer but not equal to the observed EFG. To reproduce the observed EFG's based on

TABLE I. Quadrupole frequency, isotropic and axial Knight shifts, and room-temperature spin-lattice relaxation times for each Al site in the materials studied.

	Al_3Ti		Al_3V		Al_3Nb		Al_3Ta	
Site	I	II	I	II	I	II	I	II
ν_q (MHz)	1.664	0.495	1.72	0.375	2.12	0.566	2.3	0.475
K_{iso} (%)	0.041	0.027	-0.017	-0.010	0.035	0.026	0.058	0.054
K_{ax} (%)	0.020	-0.004	0.028	0.008	0.058	-0.005	0.080	0.015
T_1 (s)	0.08±0.01	0.31±0.04	0.14±0.05	0.22±0.03	0.9±0.3	1.6±0.4	1.3±0.3	2±0.4
T_1T (s K)	24±4	92±12	41±14	64±9	261±87	464±117	377±87	580±117

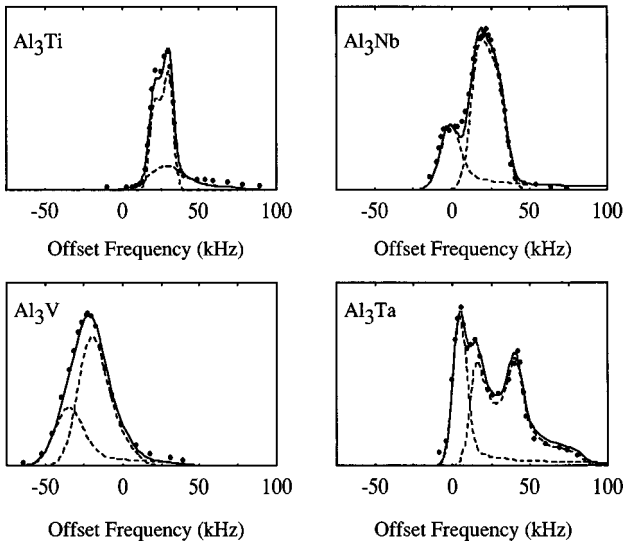

FIG. 3. Central transition ^{27}Al NMR line shapes measured in Al_3Ti, Al_3V, Al_3Nb, and Al_3Ta at room temperature. Dashed curves from numerical simulations for each Al site described in the text.

localized point charges for each ion, we found that unreasonable charge transfers were required: transition-metal atoms were required to transfer between 2.7 and 3.9 electron charges to Al, while the electronegativities for these atoms are almost identical (and unequal *s*-, *p*-, and *d*-electron transfer on this scale is unlikely). Thus it is clear that valence charges are a significant source of the observed EFG's. We attribute the large enhancement of the site I EFG to a concentration of bonding charge in the *ab* planes. This confirms the importance of *p*-*d* hybridization between Al site I and the transition metal for the structural properties of these materials.

The central transition ($m=\frac{1}{2}\leftrightarrow-\frac{1}{2}$) is more complicated because of the simultaneous presence of quadrupole and anisotropic Knight-shift effects. The room-temperature experimental powder patterns for the central transition lines are given in Fig. 3. For Al_3X alloys, the ^{27}Al quadrupole shift and the angle-dependent Knight shifts are axial due to the aluminum site symmetry. Hence the frequency shift for the central transition, $\Delta\nu$, to the second-order quadrupole interaction and Knight shift is[15]

$$\frac{\Delta\nu}{\nu_o}=\frac{K_{\rm ax}}{1+K_{\rm iso}}(3\cos^2\theta-1)+\frac{\nu_q^2}{2\nu_o^2}(1-\cos^2\theta)\times(1-9\cos^2\theta), \quad (1)$$

where ν_o is the Larmor frequency, $K_{\rm iso}$ the isotropic Knight shift, $K_{\rm ax}$ the axial Knight shift, and θ the angle between the crystal symmetry axis and the external magnetic field. Shape function fitting for the case of combined quadrupole and axial shift interactions was presented first by Jones *et al.*[16] By substituting the determined ν_q's and tuning $K_{\rm ax}$, the positions of shoulders and singularities of the polycrystalline NMR spectrum can be found. We obtained good agreement for all materials using this method. The best-fit curves drawn as dashed lines are also shown in Fig. 3. The corresponding room-temperature values for $K_{\rm ax}$ and $K_{\rm iso}$ thus obtained are listed in Table I. The curve-fits were evaluated by eye, and the values in Table I were used to produce the curves in Fig. 3, however, the last digit quoted for $K_{\rm iso}$ and $K_{\rm ax}$ in the table make very little difference for the shape of the curves. Note that in these fits we constrained the line-shape areas for site I and site II by the 1 to 2 ratio according to their occupations in DO_{22}.

TABLE II. Calculated Fermi-level *s* DOS (in units states/eV atom) for each Al crystallographic site, deduced from the NMR T_1T's.

Alloy	Site I	Site II	Total
Al_3Ti	0.0182	0.0093	0.0123
Al_3Nb	0.0055	0.0041	0.0046
Al_3Ta	0.0046	0.0037	0.0040

From the relationship of the isotropic Knight shift to the *s* DOS in metals,[17] the small $K_{\rm iso}$ for all compounds implies low DOS at the Fermi surfaces, predicted previously.[7,8] Also the larger $K_{\rm iso}$ occurring at site I indicates more *s* electrons at this site. However, $K_{\rm iso}$ is not entirely due to *s*-like conduction electrons because of *s*-*d* mixing and chemical shifts, described below. Though those terms are usually much smaller than the *s*-contact Knight shift in metals, they become competitive when the latter is significantly small. This is more obvious from the Al_3V shifts (Table II): the negative Knight shift for this material cannot be accounted for either by an ordinary *s*-contact term or by a paramagnetic orbital shift. A negative Knight shift was also found for dilute alloys of Al in V.[18] In that study, the negative term was attributed to core polarization, but the core-polarization term for 3*p* electrons is now generally agreed to be positive,[19] and too small to account for the shifts observed here. Yokoyama *et al.* noted that direct exchange polarization of *s* electrons by V-based *d* states may account for the negative shift.[20]

In further investigations, we examined the temperature dependence of the ^{27}Al central lines between room temperature and 77 K. The Al_3V line was observed to shift to lower frequencies (more negative K) at lower temperatures, while that of the other materials changed little. This agrees with the observation of a Curie-Weiss susceptibility in Al_3V.[21] The negative ^{27}Al shift corresponds to a negative Al spin polarization due to local moments on V, and our observations confirm the existence of bulk magnetism in this material (also indicated by the increased ^{27}Al NMR linewidths in Al_3V).

We have not carried out the full line-shape analysis at all temperatures, however the center of the Al_3V line shifts by $\Delta K=-0.015\%$ between room temperature and 77 K. The temperature dependence appears closer to linear than expected based on the observed Curie-Weiss behavior with $T_N=-65$ K.[21] However, extrapolating to high temperatures it is clear that the Al_3V Knight shift, with local-moment contributions removed, is near zero, and much lower than those of the other materials (Table I).

The anisotropic Knight shift, $K_{\rm an}$, is due to two terms: the spin dipolar interaction and paramagnetic (orbital) shift (the direct spin-contact interaction is isotropic). In an environment of axial symmetry, $K_{\rm an}=\frac{1}{2}K_{\rm ax}=\frac{3}{2}(K_c-K_{ab})$, with K_c

and K_{ab} corresponding to the Knight shifts in the c direction and in the ab plane, respectively. In these materials, larger $K_{\rm ax}$ occurs at site I (see Table I), while we consistently observed a smaller $K_{\rm ax}$ on site II.

For the orbital shift, there is the general form[16]

$$\sigma^P=\frac{2e^2}{m^2c^2}\sum\frac{\langle\Psi|L_z|\Psi'\rangle\left\langle\Psi'\left|\frac{L_z}{r^3}\right|\Psi\right\rangle}{\Delta E}+\text{c.c.}, \qquad (2)$$

where the Ψ is an occupied state, and the sum is over excited states Ψ'. In a tight-binding picture, the sum will also go over local orbitals making up the electron states; the first matrix element in Eq. (2) will include both local orbitals and those of neighboring sites, giving local and nonlocal contributions similar to the formalism of Pople for molecules.[22] Important contributions will come from local Al-p orbits, as well as transition d orbits from neighboring sites. Al p_x, p_y, and p_z orbits have zero matrix elements when aligned with their axes along the applied field, so the large paramagnetic sign for site I $K_{\rm ax}$ with the field along the c axis is expected for a concentration of bonds for site I in the ab plane. The nonlocal contribution for site I will also be positive for d_{xy} or $d_{x^2-y^2}$ orbitals that extend in the basal plane, as can readily be established. Thus the large site I axial Knight shifts are consistent with strong directional bonding in this plane, as also indicated in the EFG results. Correspondingly, the weaker $K_{\rm ax}$ for site II implies little directional bonding on this site.

The orbital shift term also contributes to $K_{\rm iso}$, as mentioned above, and this contribution is large in these materials, given the small contact Knight-shift contribution implied by the observed Korringa T_1's. For instance, most of the isotropic shift in Al_3Ta (0.058% for site I) must be orbital. Comparing to other ^{27}Al shifts in solids, for example the zinc-blende semiconductors with shifts in the range $+0.007\%$ to $+0.014\%$,[23] we see that the aluminide orbital shifts are unusually large. This can generally be explained by the presence of the d electrons, since the Al orbital susceptibility will be enhanced to the extent that Al-p orbitals participate in the relatively narrow d bands, and also due to a nonlocal orbital shift term. A preliminary Knight-shift study on Al_3Zr and Al_3Hf in the DO_{23} structure also agrees with this interpretation.[24]

IV. SPIN-LATTICE RELAXATION

The spin-lattice relaxation time (T_1) measurements were carried out using the inversion recovery method. We recorded the signal strength by integrating the spin echo FFT. Since the rf rotating field was applied with an amplitude of about 70 kHz, we could not separate the T_1's of individual sites from the central transition signals, where the site splitting is typically less than 30 kHz. For this reason, we found each T_1 by centering the resonance frequency at the $m=-\frac{1}{2}\leftrightarrow-\frac{3}{2}$ quadrupole-split powder pattern edges, where the resonance is dominated by one site. T_1 values were obtained by fitting to the theoretical multiexponential recovery curve, with an uncertainty less than 10%. For $m=-\frac{1}{2}\leftrightarrow-\frac{3}{2}$ transitions, we have[25]

$$\frac{M(t)-M(0)}{M(0)}=-2(0.157e^{-(t/T_1)}+0.054e^{-(3t/T_1)}+0.075e^{-(6t/T_1)}+0.446e^{-(10t/T_1)}+0.268e^{-(15t/T_1)}, \qquad (3)$$

derived from the initial conditions used in our experiments. The determined room-temperature T_1's are approximately several hundred to a thousand milliseconds, enumerated in Table I. While nonconduction mechanisms may contribute to the relaxation, these were excluded by the Korringa relation[26] in all materials except Al_3V. T_1 measurements at 77 K yielded constant T_1T indicating a conduction-electron mechanism for the relaxation.

We found that T_1T for Al_3V at 77 K and room temperature closely satisfied $T_1T\sim\sqrt{T-T_N}$, using $T_N=-65$ K as given by the susceptibility study.[20] This curve is expected for weakly antiferromagnetic metals,[27] and the results indicate that local moments dominate the relaxation processes. Subtracting the local-moment contribution leaves a very small background rate, probably indicating that the Al-s electrons are strongly coupled, leaving no separate channel for Al-s conduction-band relaxation. We plan further investigations of the magnetism of this material, particularly the apparent discrepancy between the Knight shift and bulk susceptibility.

In nonmagnetic materials, the spin-lattice relaxation time is known as a direct probe for changes of the Fermi surface. The relaxation of nuclei in a metal is dominated by their coupling to the spin magnetic moments of the s-character electrons. In these materials, the orbital contribution will be small. Based on the free-electron approximation, the spin-lattice relaxation rate can be written as[28]

$$\frac{1}{T_1T}=\frac{4\pi k_B}{\hbar}[\gamma_nH_s^{\rm HF}g_s(\epsilon_F)]^2, \qquad (4)$$

where $H_s^{\rm HF}$is the hyperfine field of the s electrons, $g_s(\epsilon_F)$ is the s DOS at the Fermi level, and γ_n is the gyromagnetic ratio. The T_1's we found to be much longer than that of the Al metal, which is about 6 ms at room temperature.[29] The long T_1 is related to DOS reduction at the Fermi level, which has been suggested to account for the DO_{22} phase stability.[7–10]

For the aluminum atom, the states near the Fermi level are predominately s and p like, the mixture of d states being rather small. Since p and d hyperfine fields are generally an order of magnitude smaller than s hyperfine fields, the main hyperfine field in such alloys arise from contact electrons. With the estimate of $H_s^{\rm HF}\sim1.9\times10^6$ G in Al metal[19] and experimental T_1T's, the Fermi-level DOS of s electrons can be obtained from Eq. (4). Universally small Fermi-surface densities of states are found, with the results shown in Table II. In addition, higher s DOS at the Fermi surface occurring at site I implies that more s electrons exist at that site, consistent with our Knight-shift measurements, which also exhibited the larger $K_{\rm iso}$ always at site I. We expect this discussion to be valid for other alloys in the DO_{22} structure. Also, previous calculations predicted that the stability of the DO_{22} structure increases rapidly as the transition-metal

d-electron count increases,[7] which has been demonstrated since the Fermi-level DOS is lower in Al_3Nb and Al_3Ta than that in Al_3Ti.

We thus have a consistent picture of the NMR features of these alloys, providing local experimental evidence for their electronic structural properties. The Knight shifts together with relaxation times provide a measure of $g(\epsilon_F)$ and an indication of orbital weights. There is some evidence that $g(\epsilon_F)$ correlates with the stability of the materials. We also have discussed the observed EFG's and tensor shifts, which are consistent with a bonding configuration in the ab plane involving Al site I and the transition metals. A strong similarity was observed for the NMR characteristics of these materials, pointing to a uniformity in the electronic structure properties. Finally, identifying the characteristic site-specific NMR signatures will allow future study of more complicated microstructures for these and related materials.

V. CONCLUSIONS

In summary, we have measured the quadrupole splittings, Knight shifts, and spin-lattice relaxation times for both crystallographic sites in Al_3Ti, Al_3V, Al_3Nb, and Al_3Ta. The small Knight shifts and long T_1's are consistent with low DOS at the Fermi surfaces in DO_{22}. The larger K_{ax} and ν_q at site I gives a concise view for the strong directionality in bonding that is believed to lead to brittleness in such alloys.

ACKNOWLEDGMENTS

We are grateful to D. G. Naugle and D. D. Rathnayaka for their help with the sample preparation. This work was supported by Texas A&M University.

*Electronic address: c0l9877@acs.tamu.edu
†Electronic address: jhross@tamu.edu

[1] J. H. Schneibel, P. F. Becher, and J. A. Horton, J. Mater. Res. **3**, 1272 (1988).
[2] M. Asta, D. de Fontaine, M. Van Schilfgaarde, M. Sluiter, and M. Methfessel, Phys. Rev. B **46**, 5055 (1992).
[3] M. Asta, D. de Fontaine, and M. Van Schilfgaarde, J. Mater. Res. **8**, 2554 (1993).
[4] C. Amador *et al.*, Phys. Rev. Lett. **74**, 4955 (1995).
[5] P. Ch. Sahu *et al.*, Phys. Rev. Lett. **78**, 1054 (1997).
[6] W. B. Pearson, *A Handbook of Lattice Spacings and Structures of Materials and Alloys* (Pergamon, Oxford, 1967); *Structure Reports* (International Union of Crystallography, Utrecht, 1967), Vol. 32, Pt. A, p. 14.
[7] A. E. Carlsson and P. J. Meschter, J. Mater. Res. **4**, 1060 (1989).
[8] T. Hong *et al.*, Phys. Rev. B **41**, 12 462 (1990).
[9] J. H. Xu and A. J. Freeman, Phys. Rev. B **41**, 12 553 (1990).
[10] Senying Liu, Rongze Hu, and Chongyu Wang, J. Appl. Phys. **74**, 3204 (1993); **79**, 214 (1996).
[11] H. Okamoto, J. Phase Equilibria **14**, 120 (1993).
[12] Jianhui Shi, James Chepin, and Joseph H. Ross, Jr., Phys. Rev. Lett. **69**, 2106 (1992).
[13] James Chepin and Joseph H. Ross, Jr., in *Determining Nanoscale Physical Properties of Materials by Microscopy and Spectroscopy*, edited by M. Sarikaya, H. K. Wickramasinghe, and M. Isaacson, MRS Symposia Proceedings No. 332 (Materials Research Society, Pittsburgh, 1994), p. 267.
[14] C. Berthier and M. Minier, J. Phys. F **7**, 515 (1977).
[15] M. H. Cohen and F. Reif, *Solid State Physics* (Academic Press, New York, 1957), Vol. 5, p. 11.
[16] W. H. Jones, Jr., T. P. Graham, and R. G. Barnes, Phys. Rev. **132A**, 1898 (1969).
[17] C. P. Slichter, *Principles of Magnetic Resonance* (Springer-Verlag, New York, 1990).
[18] D. O. Van Ostenburg *et al.*, Phys. Rev. **135A**, 455 (1964).
[19] G. C. Carter, I. D. Weisman, and L. H. Bennett, Phys. Rev. B **5**, 3621 (1972).
[20] N. Yokoyama *et al.*, J. Phys. Soc. Jpn. **37**, 73 (1974).
[21] L. Creveling, Jr. and H. L. Luo, Phys. Lett. **28A**, 772 (1969).
[22] J. A. Pople, Proc. R. Soc. London, Ser. A **239**, 541 (1957).
[23] R. E. J. Sears, Phys. Rev. B **22**, 1135 (1980); Oc Hee Han, Hye Kyung C. Timken, and Eric Oldfield, J. Chem. Phys. **89**, 6046 (1988).
[24] Chin-Shan Lue and Joseph H. Ross, Jr. (unpublished).
[25] W. W. Simmons, W. J. O'Sullivan, and W. A. Robinson, Phys. Rev. **127**, 1168 (1962).
[26] J. Korringa, Physica (Utrecht) **16**, 601 (1950).
[27] Toru Moriya, *Spin Fluctuations in Itinerant Electron Magnetism* (Springer-Verlag, Berlin, 1985).
[28] A. Abragam, *Principles of Nuclear Magnetism* (Oxford University Press, Oxford, 1982).
[29] J. J. Spokas and C. P. Slichter, Phys. Rev. **113**, 1318 (1959); A. G. Anderson and A. C. Redfield, *ibid.* **116**, 583 (1959).